Selma Schmidt, Max Wiebicke, Ivo Herle

On the determination and evolution of fabric in representative elementary volumes for a sand specimen in triaxial compression

Erstveröffentlichung in / First published in:

Granular matter. 2022, 24 (4), Art.-Nr. 97 {Zugriff am: 03.11.2022}. Springer. ISSN 1434-7636.

DOI: http://dx.doi.org/10.1007/s10035-022-01262-2

Granular Matter (2022) 24:97
https://doi.org/10.1007/s10035-022-01262-2

BRIEF COMMUNICATION

On the determination and evolution of fabric in representative elementary volumes for a sand specimen in triaxial compression

Selma Schmidt[1] · Max Wiebicke[1,2] · Ivo Herle[1]

Received: 7 March 2022 / Accepted: 8 July 2022

Abstract
The soil response in triaxial compression tests, that are commonly treated as element tests, is known to be inhomogeneous. Several studies have revealed the localisation of deformation throughout the whole specimen by digital image correlation techniques on X-ray tomographies. The fabric of a soil specimen has so far only been studied on complete specimens as a bulk measurement or in chosen subsets. In this contribution, we present a study on the spatial and temporal distribution of the fabric throughout one Hostun sand sample in triaxial compression. Therefore, we calibrated the minimum representative element size first for three chosen fabric variables considering three different criteria. By distributing the elements in a regular grid over the specimen, we are able to clearly identify the onset of the localisation in terms of void ratio, coordination number and contact fabric anisotropy. Spatially and temporally the contact fabric variables precede the void ratio changes as they are much more sensitive to small changes.

Keywords REV · Fabric · Heterogeneity · Sand · X-ray CT · Inter-particle contacts

1 Introduction

For many decades, soils have been modelled as a continuum by means of phenomenological equations. The common approach to determine the soil properties embedded in these equations is the use of so called element tests. In these tests, we seek to find the elementary soil response and therefore assume the specimen to behave homogeneously. As a result, we interpret the test results measured at the boundary of the specimen as representative of the complete specimen. This is in strong contrast to several phenomena, such as strain localisation, that can be observed during these element tests and have been analysed many times, especially since the rise of x-ray computed tomography (CT), *e.g.* [1, 2].

One of the first applications of such full-field measurements of specimens were the scans by Desrues et al. [3], which revealed the heterogeneity of the density in a sheared sand sample. It has been shown that this heterogeneity is present even when not observable from the outside, since a complex pattern of shear bands can form inside the specimen. In a recent study, Desrues et al. [4] revisited the original experiments with newly-developed techniques allowing for the detection of small strain localisation. The most shocking finding is probably that *"there does not appear to be a single moment where strain localisation starts"*. This leads to further questioning the assumption of homogeneity as the soil seems to behave heterogeneously from very early on.

Especially in terms of kinematics, the heterogeneous answer of the soil has been studied extensively over the past decade using tools such as the digital image correlation (DIC) combined with microfocus x-ray CT (μCT) [5–7]. There has also been an attempt to connect the kinematic heterogeneity with the evolution of force chains inside the specimen, *e.g.* [8]. It has been observed that force chains, which develop under loading, buckle inside

Max Wiebicke and Ivo Herle contributed equally to this work.

✉ Selma Schmidt
selma.schmidt@tu-dresden.de

Max Wiebicke
max.wiebicke@sydney.edu.au

Ivo Herle
ivo.herle@tu-dresden.de

[1] Institut für Geotechnik, Technische Universität Dresden, George-Bähr Strasse 1a, Dresden 01069, Saxony, Germany

[2] Sydney Centre in Geomechanics and Mining Materials, School of Civil Engineering, The University of Sydney, Sydney 2006, Australia

Published online: 09 August 2022

the shear band when approaching the critical state. Furthermore, there have been approaches combining x-ray CT with x-ray diffraction [9, 10]. While the former allows for the investigation of *e.g.* particle kinematics or contact characteristics, the latter allows for the measurement of particle-averaged lattice strain. The combination of the two methods can ultimately lead to the quantification of interparticle forces as described in [9]. The heterogeneity of the soil has additionally been studied regarding particle breakage [10–12]. The findings of those studies mainly correspond to the ones above as a significant amount of breakage seems to be happening inside the shear band.

Generally, it can be concluded that most of the globally observed soil behaviour takes place inside the localisation zone. Already several years ago, it has been shown [3] that a unique critical state is, in fact, only reached inside the shear band due to the localisation of shear in this region. This gives a general idea about possible consequences arising from the consideration of the specimen as a homogeneous element and the use of this assumption for the soil model calibration. Even more complex problems arise once a specimen containing a pattern of shear bands is considered. Wood [13] discusses this issue amongst other difficulties with respect to heterogeneous responses in soil testing and their consideration in soil modelling.

Several studies have determined representative elementary volumes (REV) specifically for the void ratio or the porosity for different sands using x-ray μCT. The REV sizes for Ottawa sand, a sub-rounded sand, range from 4.2 [14, 15] to 5.7 d_{50} [16]; the REV sizes for spherical or close to spherical sand grains range from 2 [11, 15] to 5 d_{50} [17]. Given that all specimens studied in these contributions have a narrow grain size distribution, the difference should mostly be due to the grain shape and a tendency of increasing REV size for increasing angularity can be observed.

The above mentioned investigations already show that the behaviour of soils is by no means homogeneous, but for a more complete micro-mechanical analysis at the grain-scale, the fabric of the material has to be included. The fabric was already analysed with x-ray CT in various contributions either globally on the complete specimen [18] or locally in specific subvolumes or cores [1, 19]. Observations of the contact fabric evolution in different regions of two soil specimens in [20] showed a different development inside and outside the emerging shear band.

In this study, μCT scans of a specimen in triaxial compression are investigated regarding its fabric. The heterogeneity of the soil is analysed on the spatial and temporal scale. For this purpose, the size of the REV is determined for each variable and the specimen is examined using these REVs.

2 Image analysis

The triaxial compression test presented here considers a pluviated and initially dense Hostun sand specimen with a very narrow grain size distribution and an average grain diameter of $d_{50} = 338\mu$m. The specimen has been tested at 100 kPa cell pressure. The test was carried out in the x-ray scanner in Laboratoire 3SR in Grenoble in order to acquire 13 μCT images during the loading. The macroscopic response of the sample can be seen in Fig. 1. Only 7 scans are clearly visible in the plot, as the experiment comprises unloading and reloading curves with very small changes to void ratio and the contact fabric. The tomographies are analysed with the techniques presented and studied in [21] using the open source software *spam* [22] to determine the contact fabric.

The experiment and the image analysis of the bulk specimen are described in detail in [23]. The μCT images have a voxel size of 15 μm, which leads to the specimen containing $\approx 730 \times 730 \times 1470$ voxel. To obtain the contact fabric from every μCT scan, the images are first binarised by a global threshold and then segmented by a topological watershed. To enhance contact detection, a local threshold is introduced and for a better characterisation of the contact plane, a power watershed, namely the random walker, is applied to every contact. This allows for the determination of the contact plane on a sub-pixel level. For the computation of the contact orientation, which is the orientation of the contact normal, a PCA is performed.

This results in a second order fabric tensor **N** describing the contact orientations of the entire specimen.

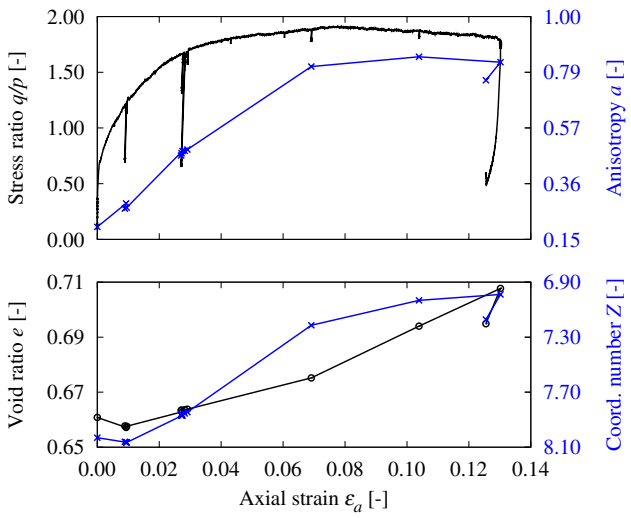

Fig. 1 Macroscopic response of the Hostun sand sample to triaxial compression. The fabric variables anisotropy a and coordination number Z are plotted in blue

$$\mathbf{N} = \frac{1}{N}\sum_{\alpha=1}^{N} \mathbf{o}^{\alpha} \otimes \mathbf{o}^{\alpha} \tag{1}$$

with N being the number of orientations and **o** being one individual orientation. As in the previous publications, the contact fabric is described by two scalar variables: the coordination number Z and the contact fabric anisotropy a. The coordination number represents the average number of contacts per grain.

$$Z = \frac{2 \cdot N_c}{N_p} \tag{2}$$

with N_c being the number of contacts and N_p being the number of particles. The contact fabric anisotropy is calculated from the deviatoric part of the fabric tensor **D**.

$$a = \sqrt{\frac{3}{2}\mathbf{D} : \mathbf{D}} \tag{3}$$

These two variables are also plotted in Fig. 1 for the complete specimen.

In this contribution, we will extract information for small subsets within the specimen in order to study the spatial distribution of the fabric. Therefore, it is important to define the set of contacts that is to be analysed. In this work, we consider all grains whose centre of mass is located in a specified window as internal grains and those contacting these, yet their centre of mass is outside the specified window, as external grains. Contacts between internal grains are considered twice and contacts between internal and external grains are considered once in the calculation of the coordination number. The overall contact fabric of the complete specimen is computed in a similar way. As the latex membrane is barely identifiable, the outermost particles are considered as the boundary of the complete specimen.

3 Representative elementary volume

The size of a REV is generally described as the smallest possible volume for which a chosen variable is independent of the size of the volume [24]. Throughout the analysed triaxial compression test, we observe different regions forming inside the specimen, the most obvious ones being a zone of localisation as well as the regions above and below. If we want to analyse the properties and behaviour of those regions, it is crucial that the REV is sufficiently large to catch the characteristics of each region while being as small as possible, such that the different regions can be distinguished. The REV is, in this case, representative of the specific region inside the specimen and not representative of the specimen on the whole.

In order to define this size, cubic volume elements of increasing size are extracted from four different positions (y = 400, 600, 800, 1000) along the vertical centre axis of the specimen for the states of the loading shown in Fig. 1. The positions were chosen so that even the largest investigated element size remains unaffected by boundary effects and they are fixed for the complete analysis. Figure 2 shows chosen element sizes that are investigated to find the REV size as well as some characteristic positions along the vertical centre axis of the specimen. This information is displayed on an image of the specimen showing incremental grain rotations to highlight the position of the emerging shear band. Figure 3 shows the positions from which elements are extracted for one of the element sizes and three different loading states. The contact fabric in these elements is extracted from the overall fabric of the specimen, *i.e.* global lists of contacts and orientations. Therefore, the particles whose centre of mass is located within the volume are identified and their contacts are collected. This includes contacts to other particles within the element, but also to the surrounding particles as described above. The variables that are determined for each of the volumes are the void ratio, the coordination number and the contact fabric anisotropy.

The main criteria for determining the REV size are the convergence of the empirical mean μ and the variance σ^2 of the selected variables with increasing element size. The values for each variable should converge at each position, but do not need to be identical throughout the sample as we expect a slight heterogeneity already at the initial state. The REV should not be representative of the whole sample, but rather of the analysed zone. Furthermore, a χ^2

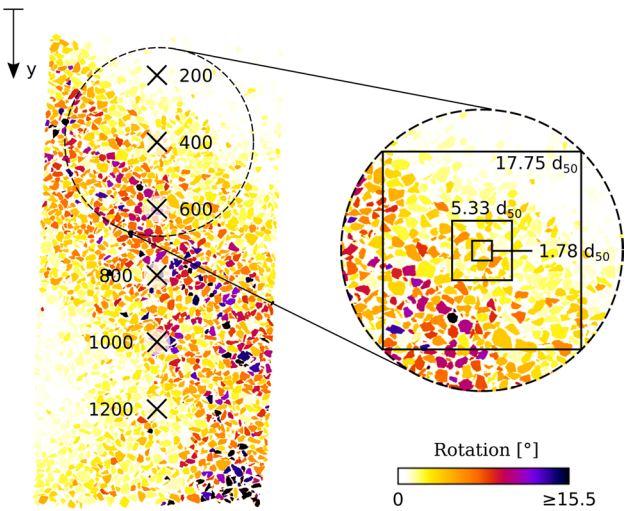

Fig. 2 Incremental rotation of individual grains from 2.9% to 6.9% of axial strain. These measurements are acquired using the DDIC scripts from *spam* [22]. The zoom visualises the minimum and maximum size of the elements for the REV study as well as the REV size determined for the contact fabric

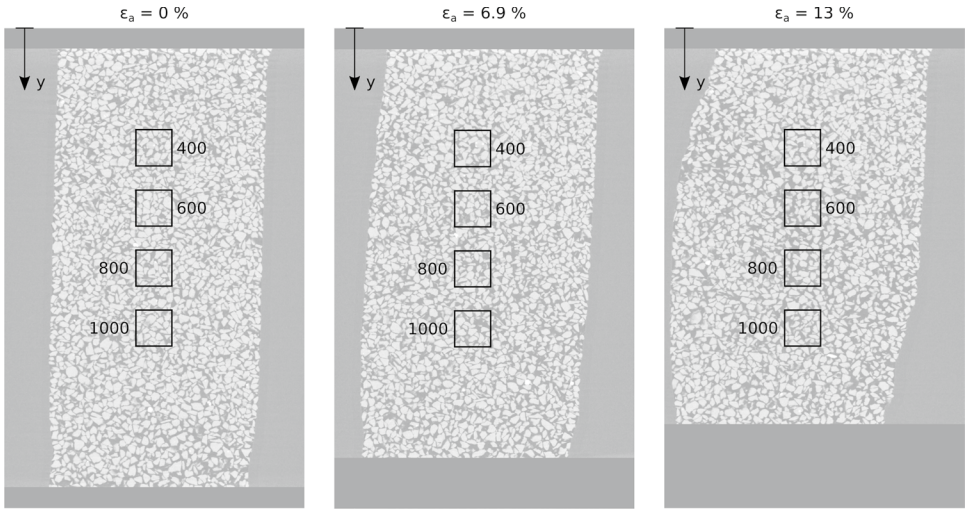

Fig. 3 Elements at the four locations used for the study of the REV size shown for three loading states. The element size equals the REV size determined for the contact fabric

test as described in [25] is added as a criterion for the determination of the REV size. This test is usually used in statistical analysis to determine whether an unknown distribution function is of a certain type. This approach is now modified so that the value of each element is compared to the mean value of all analysed elements of that size. The χ^2 test introduces a critical value for a chosen accuracy or respectively a chosen variation from the mean value. As the variation changes drastically once localisation starts, this value has to be calibrated twice – for all images before and after the onset of localisation. Both critical values are calibrated on one of the images and applied to the other ones. Further information on the calibration and implementation of the χ^2 test can be found in the Appendix. The same critical value is used for all three soil variables. The convergence criteria and the χ^2 criteria are evaluated for each individual variable and for the increasing element size.

Figure 4 shows the results of the analysis for the initial state. All three variables converge with increasing element size. The lower row shows that the variance as well as the χ^2 value decrease rapidly for the void ratio as well as the coordination number and slower for the anisotropy. It can also be observed that the mean and/or the variance might sometimes need a larger REV size to converge than the one suggested by the χ^2 test. For instance, when analysing the

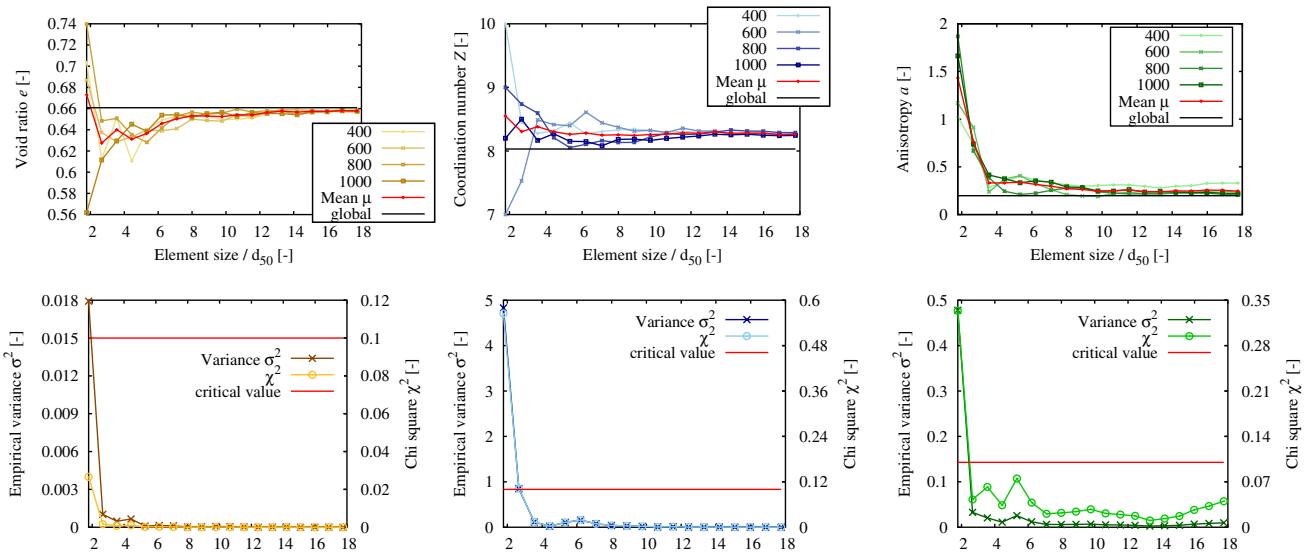

Fig. 4 Determination of the REV size at the initial state for the fabric descriptors void ratio, coordination number and contact fabric anisotropy. The REV size is expressed as the side length of the cube normalised by the average grain diameter of Hostun sand. The criteria for determining the REV size are the convergence of the mean and the variance plus a χ^2 test. The global value in black is calculated on the complete specimen

convergence of the mean anisotropy, it is clearly visible that it only converges for an element size of 3.55 d_{50} while the χ^2 test would lead to a REV size of 2.66 d_{50}. There are also loading states for which the χ^2 test gives a higher REV size than the convergence. The REV size needs to be chosen so that small scale fluctuations are eliminated while, at the same time, the REV remains as small as possible. Thus, we use the largest size necessary for defining the minimum element size from all three criteria.

As already pointed out in [26], the size of the REV depends on the chosen variable. The minimum edge length of the cubic element is 2.66 d_{50} for the void ratio and 3.55 d_{50} for the coordination number and the anisotropy at the initial state. These sizes were evaluated over all the images (states) with the results being summarised in Table 1. The results are also presented in Figure 5. A correlation between the evolution of the REV sizes and the evolution of the test can be observed to some extend with the REV size of the coordination number being far more sensitive to the load reversals than the REVs of the other two variables. The minimally necessary sizes considering all images are 3.55 d_{50} for e and 5.33 d_{50} for Z and a. Note that this analysis is carried out based on the actual size of the elements and not on the number of particles in these elements. The specimen is initially dense which corresponds to a range of 30-50 particles with their centre of mass inside the investigated elements of the size 3.55 d_{50} and 115-155 particles for 5.33 d_{50}.

The minimal REV size determined for the void ratio is slightly lower than can be expected based on the range of sizes given in the literature as introduced above. For spherical particles the sizes ranged from 2 [11, 15] to 5 d_{50} [17] while they ranged from 4.2 [14, 15] to 5.7 d_{50} [16] for sub-rounded particles, indicating even larger sizes for the angular particles presented in this study. This was not confirmed, as the REV size for e was determined to be 3.55 d_{50}.

Table 1 Edge lengths of the determined REVs for each of the analysed images and chosen variables. Superscripts refer to the criteria leading to this size: 1 ... χ^2 test, 2 ... convergence of the mean, 3 ... convergence of the variance

Image	Void ratio [d_{50}]	Coord. number [d_{50}]	Anisotropy [d_{50}]
1	2.66^{3}	$3.55^{1,3}$	3.55^{2}
2	2.66^{3}	$2.66^{1,3}$	$4.44^{1,3}$
3	2.66^{3}	$4.44^{2,3}$	$\mathbf{5.33}^{1}$
4	2.66^{3}	3.55^{3}	$\mathbf{5.33}^{1,3}$
5	$\mathbf{3.55}^{3}$	$\mathbf{5.33}^{2,3}$	$4.44^{1,3}$
6	$\mathbf{3.55}^{3}$	$3.55^{1,3}$	$4.44^{1,3}$
7	$\mathbf{3.55}^{3}$	$3.55^{1,3}$	$4.44^{1,3}$
8	$\mathbf{3.55}^{3}$	$3.55^{1,3}$	$4.44^{1,3}$
9	$\mathbf{3.55}^{3}$	$3.55^{1,3}$	$4.44^{1,3}$
10	$\mathbf{3.55}^{2,3}$	4.44^{1}	4.44^{1}
11	$\mathbf{3.55}^{2}$	$\mathbf{5.33}^{1}$	$4.44^{1,3}$
12	–	2.66^{1}	4.44^{1}
13	–	$2.66^{1,2,3}$	$3.55^{1,2,3}$

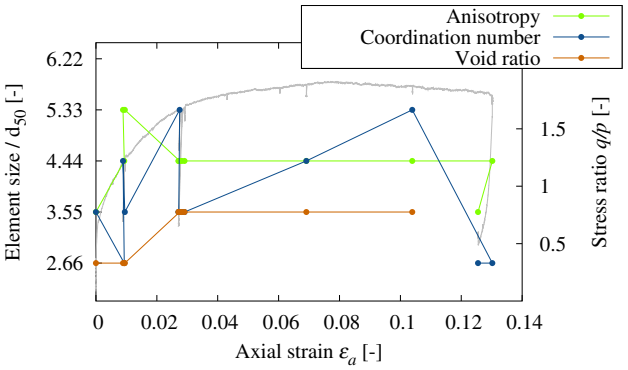

Fig. 5 Evolution of the REV sizes determined at each loading state for the chosen variables compared to the evolution of the test

4 Evolution of contact fabric in the REVs

To study the distribution of fabric variables for the complete specimen, the elements are placed in a regular grid throughout the specimen. The distance of the centre of the elements to each other is 2.22 d_{50}, which means that the elements are overlapping in order to extract information on a fine grid. Elements located along the boundary of the specimen are only partially filled with grains. Thus, we need to define a threshold to exclude elements from this analysis in order to agree with the requirement of counting as a REV. For the contact fabric, a threshold of 90 particles is chosen to exclude elements placed on the boundaries of the specimen. This corresponds to the minimum number of particles found in a single REV (with respect to the contact fabric) within the specimen for every loading step. Regarding the void ratio, a threshold for the specimen boundary was defined with respect to the total volume of soil, *i.e.* particles and internal voids, inside the REV. It has been chosen in accordance with observations on the convergence of the mean and variance in the REV study. The selected value corresponds to the amount of 68% of the element filled with the soil composed of particles and voids between them.

The spatial distribution of the three fabric variables is shown in Fig. 6 for the initial state and for the state at 13% axial strain. The chosen vertical slice is oriented to contain the shear band. It is clearly visible that the specimen is heterogeneous even at the initial state. After the onset of localisation, the map of the void ratio reveals a strong dilation inside the shear band, which was already shown

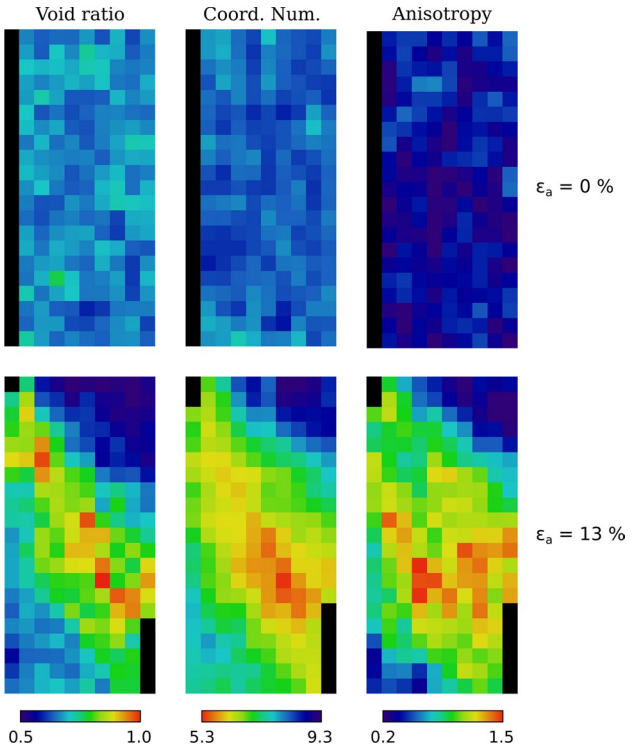

Fig. 6 Distribution of the fabric variables displayed in vertical slices at the initial state and at 13% of axial strain. The vertical slices are chosen to contain the planar shear band. The black pixels are elements without a sufficient number of particles or total volume of soil, respectively, and therefore excluded

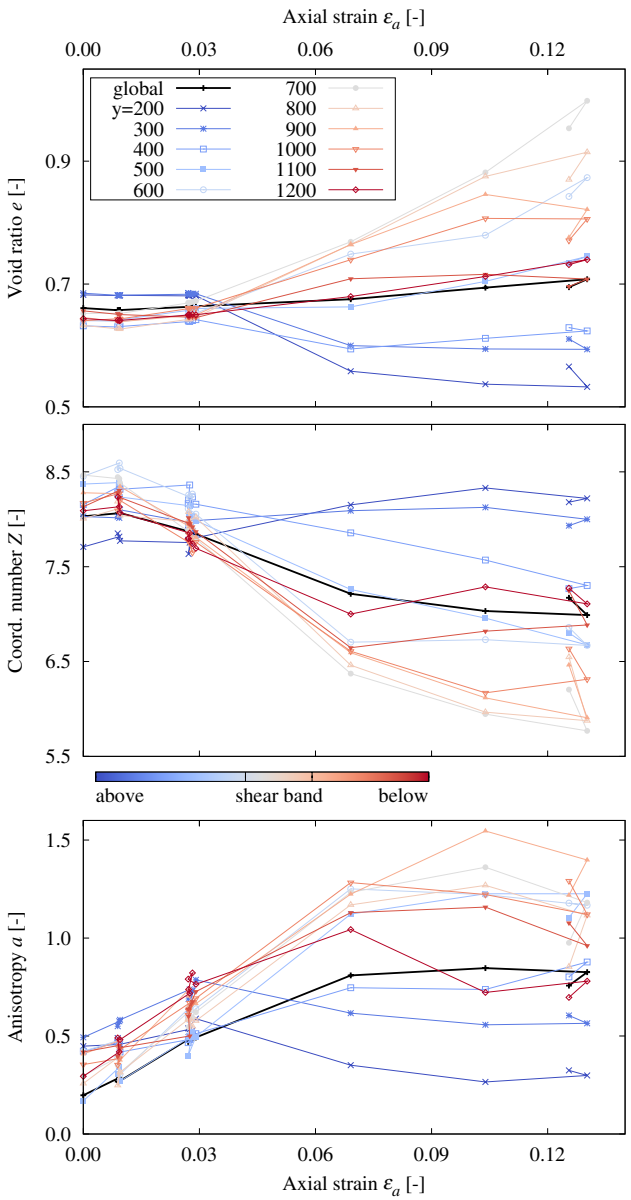

Fig. 7 Fabric evolution in chosen REVs along the vertical centre line of the specimen

in many previous contributions, see *e.g.* [1, 3, 14, 16]. The coordination number delivers a similar picture: a low number of contacts per grain inside the shear band and a higher number outside. The anisotropy is not as clearly localised in a thin band as the other two variables, but also shows a much higher magnitude inside the shear band and a lower one in the top and bottom wedges.

The localisation of both contact fabric variables is broader than of the void ratio. This shows that the contact fabric in elements close to the shear band picks up the shear localisation although the void ratio is not impacted there. Especially the anisotropy, which is not only effected by the re-orientation but also by the loss and gain of contacts, is highly sensitive to small changes inside the specimen and is therefore greatly impacted by the localisation.

A similar behaviour can also be observed on the temporal scale, see Fig. 7, which shows the evolution of chosen elements along the vertical centre axis of the specimen. At about 3% of axial strain a single shear band starts to evolve. This is clearly recognisable for all fabric variables as the individual elements start to behave very differently. The elements in the emerging shear band (located at y = 700, 800, 900) show a strong dilatancy with a loss of contacts and high anisotropy. The elements outside the shear band either behave oppositely (above) or do not evolve at all (below) once localisation starts.

Figure 8 shows the statistical evolution of all three fabric variables with the macroscopic loading. Similar to the evolution along the vertical centre line, the distribution of all variables expands starting at 3% of axial strain. Initially, there is only a small scatter of the void ratio and the coordination number whereas the anisotropy shows a larger initial heterogeneity. The coordination number picks up the change in volume well before the void ratio and much more distinctly, both in terms of the mean as well as the standard deviation.

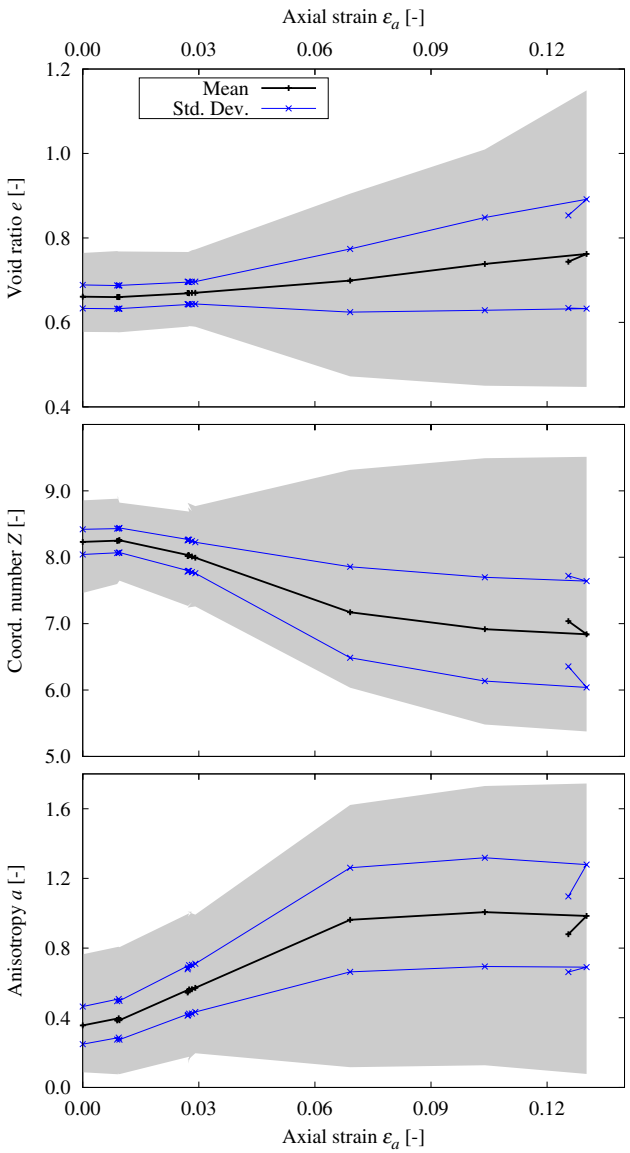

Fig. 8 Evolution of the fabric in the REVs of the complete sample. The grey background represents the min/max values of the respective entities

5 Discussion and conclusion

In this work, we present a methodology to study the spatial and temporal distribution of the void ratio, the coordination number and the contact orientation anisotropy in a sand specimen. These fabric variables are measured using x-ray CTs acquired during a triaxial compression test on the specimen. To compute the spatial distribution throughout the specimen, the minimum REV size is determined using three criteria: the χ^2 test as well as the convergence of the mean and the variance. One major finding of this study is the identification of a size for the representative cubic element with a side length of 5.33 d_{50} for the contact fabric and 115 to 155 particles inside the investigated elements.

We find that the onset of strain localisation is not only clearly visible in the void ratio, but also in the coordination number and anisotropy. We present the full field of these variables and are thus able to study the extent of the localisation of the contact fabric variables, both temporal and spatial, compared to the classic measures such as the void ratio. A further major finding is that spatial as well as temporal changes are indicated by the contact fabric before they are picked up by the void ratio. The localisation of the contact fabric is also wider than of the void ratio, showing that it is sensitive to small changes and picks these up early.

It has to be noted that the presented results on the REV size for the geometric fabric variables and their distribution are limited to one test on an initially dense sand with a narrow grain size distribution. Although this is only one specific analysis, it emphasises the heterogeneous response of a sand specimen in a so-called element test, which is commonly interpreted as a material point.

Considering such heterogeneous soil responses already at relatively small strains, we should rethink the interpretation of element tests as boundary value problems rather than as material points.

Appendix

A χ^2 test is conducted where, for each analysed variable, the value of each of the chosen elements a_i is compared to the mean value $\overline{a}$ of those elements. The null hypothesis would then state

$$H_0 : \ a_i = \overline{a} \ \text{ for all } i \tag{4}$$

and the alternative hypothesis accordingly

$$H_1 : \ a_i \neq \overline{a} \ \text{ for at least one } i. \tag{5}$$

The χ^2 value is calculated as

$$\chi^2 = \sum_{i=1}^{r} \frac{(a_i - \overline{a})^2}{\overline{a}} \tag{6}$$

where r is the number of chosen elements.

The null hypothesis is satisfied within a certain confidence interval if the χ^2 value is lower than a critical value corresponding to the degrees of freedom used and the chosen confidence coefficient. The degrees of freedom k depend on the number of chosen elements r as well as the number of estimated parameters m

$$k = r - m - 1. \tag{7}$$

In this case, elements were extracted from four different positions and only one parameter, namely the mean value, was estimated. This results in $k = 2$. As the confidence interval is not known, the critical value is calibrated directly on the first image by comparison with the convergence of the mean and the variance of the selected variable. This results in a critical value $\chi^2_{crit} = 0.103$ which corresponds to a confidence coefficient of $1 - \alpha = 0.05$ or, in other words, an accuracy of 0.95 or 95%. This is in accordance to the value used in [25].

After the onset of localisation, the critical value has to be re-calibrated, as a larger variation of the variables has to be considered. It is then calibrated on the 10th image where the shear band first becomes visible. The critical value is adjusted to $\chi^2_{crit} = 0.211$ which corresponds to a confidence coefficient of $1 - \alpha = 0.10$ or an accuracy of 0.90 or 90%.

Acknowledgements We express our thanks to Pascal Charrier, Edward Andò and Gioacchino Viggiani from Laboratoire 3SR for the allocation of time of the x-ray CT scanner and the technical support accompanying such measurements. We thank the Center for Information Services and High Performance Computing (ZIH) at TU Dresden for generous allocations of computing resources.

Funding Open Access funding enabled and organized by Projekt DEAL. The research leading to these results has received a partial funding from the German Research Foundation (DFG) Grant No. 254872581 and 453596084 (SFB/TRR 339).

Declarations

Conflict of interest The authors declare that they have no conflict of interest.

References

1. Oda, M., Takemura, T., Takahashi, M.: Microstructure in shear band observed by microfocus X-ray computed tomography. Géotechnique **54**(8), 539–542 (2004). https://doi.org/10.1680/geot.2004.54.8.539
2. Desrues, J., Andò, E.: Strain localisation in granular media. Comptes Rendus Physique **16**(1), 26–36 (2015). https://doi.org/10.1016/j.crhy.2015.01.001
3. Desrues, J., Chambon, R., Mokni, M., Mazerolle, F.: Void ratio evolution inside shear bands in triaxial sand specimens studied by computed tomography. Gèotechnique **46**(3), 529–546 (1996). https://doi.org/10.1680/geot.1996.46.3.529
4. Desrues, J., Andò, E., Mevoli, F.A., Debove, L., Viggiani, G.: How does strain localise in standard triaxial tests on sand: revisiting the mechanism 20 years on. Mech. Res. Commun. (2018). https://doi.org/10.1016/j.mechrescom.2018.08.007
5. Hall, S.A., Bornert, M., Desrues, J., Pannier, Y., Lenoir, N., Viggiani, G., Bésuelle, P.: Discrete and continuum analysis of localised deformation in sand using x-ray μct and volumetric digital image correlation. Géotechnique **60**(5), 315–322 (2010). https://doi.org/10.1680/geot.2010.60.5.315
6. Andò, E., Hall, S.A., Viggiani, G., Desrues, J., Bésuelle, P.: Grain-scale experimental investigation of localised deformation in sand: a discrete particle tracking approach. Acta Geotech. (2012). https://doi.org/10.1007/s11440-011-0151-6
7. Druckrey, A., Alshibli, K., Al-Raoush, R.: Discrete particle translation gradient concept to expose strain localisation in sheared granular materials using 3D experimental kinematic measurements. Géotechnique **68**(2), 162–170 (2018). https://doi.org/10.1680/jgeot.16.P.148
8. Rechenmacher, A., Abedi, S., Chupin, O.: Evolution of force chains in shear bands in sands. Geotechnique **60**(5), 343–351 (2010). https://doi.org/10.1680/geot.2010.60.5.343
9. Hurley, R., Hall, S., Andrade, J., Wright, J.: Quantifying interparticle forces and heterogeneity in 3d granular materials. Phys. Rev. Lett. (2016). https://doi.org/10.1103/PhysRevLett.117.098005
10. Cil, M.B., Alshibli, K.A., Kenesei, P.: 3d experimental measurement of lattice strain and fracture behavior of sand particles using synchrotron x-ray diffraction and tomography. J. Geotech. Geoenviron. Eng. **143**(9), 04017048 (2017). https://doi.org/10.1061/(ASCE)GT.1943-5606.0001737
11. Karatza, Z., Andò, E., Papanicolopulos, S.-A., Ooi, J.Y., Viggiani, G.: Evolution of deformation and breakage in sand studied using X-ray tomography. Géotechnique **2**, 1–11 (2017). https://doi.org/10.1680/jgeot.16.P.208
12. Zhao, B., Wang, J., Andò, E., Viggiani, G., Coop, M.R.: Investigation of particle breakage under one-dimensional compression of sand using x-ray microtomography. Can. Geotech. J. **57**(5), 754–762 (2020). https://doi.org/10.1139/cgj-2018-0548
13. Muir Wood, D.: Discussion: heterogeneity and soil element testing. Geotech. Lett. **2**(4–6), 217–219 (2012). https://doi.org/10.1680/geolett.12.00059
14. Amirrahmat, S., Alshibli, K.A., Jarrar, M.F., Zhang, B., Regueiro, R.A.: Equivalent continuum strain calculations based on 3D particle kinematic measurements of sand. Int. J. Numer. Anal. Methods Geomech. **42**(8), 999–1015 (2018). https://doi.org/10.1002/nag.2779
15. Razavi, M.R., Muhunthan, B., Hattamleh, O.A.: Representative elementary volume analysis of porous media using X-ray computed tomography. Geotech. Testing J. (2007). https://doi.org/10.1016/j.powtec.2010.02.011
16. Imseeh, W.H., Alshibli, K.A., Al-Raoush, R.I.: Discrepancy in the critical state void ratio of poorly graded sand due to shear strain localization. J. Geotech. Geoenviron. Eng. **146**(8), 04020066 (2020). https://doi.org/10.1061/(asce)gt.1943-5606.0002280
17. Al-Raoush, R.I., Willson, C.S.: Extraction of physically realistic pore network properties from three-dimensional synchrotron X-ray microtomography images of unconsolidated porous media systems. J. Hydrol. **300**(1–4), 44–64 (2005). https://doi.org/10.1016/j.jhydrol.2004.05.005
18. Imseeh, W.H., Druckrey, A.M., Alshibli, K.A.: 3D experimental quantification of fabric and fabric evolution of sheared granular materials using synchrotron micro-computed tomography. Granular Matter (2018). https://doi.org/10.1007/s10035-018-0798-x

19. Fonseca, J., O'Sullivan, C., Coop, M.R., Lee, P.D.: Quantifying the evolution of soil fabric during shearing using directional parameters. Géotechnique **63**(6), 487–499 (2013). https://doi.org/10.1680/geot.12.P.003
20. Wiebicke, M., Andò, E., Viggiani, G., Herle, I.: Measuring the evolution of contact fabric in shear bands with x-ray tomography. Acta Geotechnica **15**(1), 79–93 (2020). https://doi.org/10.1007/s11440-019-00869-9
21. Wiebicke, M., Andò, E., Herle, I., Viggiani, G.: On the metrology of interparticle contacts in sand from x-ray tomography images. Meas. Sci. Technol. (2017). https://doi.org/10.1088/1361-6501/aa8dbf
22. Stamati, O., Adò, E., Roubin, E., Cailletaud, R., Wiebicke, M., Pinzon, G., Couture, C., Hurley, R.C., Caulk, R., Caillerie, D., et al.: Spam: Software for practical analysis of materials. J. Open Source Softw. **5**(51), 2286 (2020). https://doi.org/10.21105/joss.02286
23. Wiebicke, M., Herle, I., Andò, E., Viggiani, G.: Measuring the fabric evolution of sand-application and challenges. Geotechnik **44**(2), 114–122 (2021). https://doi.org/10.1002/gete.202000019
24. Al-Raoush, R., Papadopoulos, A.: Representative elementary volume analysis of porous media using X-ray computed tomography. Powder Technol **200**(1–2), 69–77 (2010). https://doi.org/10.1016/j.powtec.2010.02.011
25. Gitman, I., Askes, H., Sluys, L.: Representative volume: existence and size determination. Eng. Fract. Mech. **74**(16), 2518–2534 (2007). https://doi.org/10.1016/j.engfracmech.2006.12.021
26. Wiącek, J., Molenda, M,: Representative elementary volume analysis of polydisperse granular packings using discrete element method. Particuology **27**, 88–94 (2016). https://doi.org/10.1016/j.partic.2015.08.004